Published on 31 January 2022. Downloaded by Suzhou Institute of Nano-Tech and Nano-Bionics, Chinese Academy of Sciences on 12/12/2022 2:15:21 AM.

Journal of Materials Chemistry C

ROYAL SOCIETY OF CHEMISTRY

COMMUNICATION

View Article Online
View Journal | View Issue

Check for updates

Cite this: J. Mater. Chem. C, 2022, 10, 2945

Received 17th November 2021, Accepted 28th January 2022

DOI: 10.1039/d1tc05550j

rsc.li/materials-c

Non-fused molecular photovoltaic acceptor with a planar core structure enabled by bulky and embracing-type side chains†

Zhong-Xin Xue,[a] Jin Fang,*[b] Jia Li,[c] Di Zhang,[a] Zi-Wen Xu,[a] Li-Na Liu,[ad] Jianhua Yao,*[cd] Chang-Qi Ma[b] and Wei-Shi Li*[ad]

A strategy involving bulky and "embracing"-type side chains for keeping the planarity of non-fused units was proposed and applied to the design of a non-fullerene acceptor (NFA) molecule. The NFA molecule iPrBT-NFA bearing a 2,2′-bithiophene core with two bulky and embracing-type 2,4,6-triisopropylphenyl substituents at its 3,3′ positions was demonstrated to display a planar core structure, red-shifted light absorption, finely regulated aggregation and much better photovoltaic performance than that shown by a reference molecule (DeBT-NFA) having the same backbone but with long alkyl side chains.

Numerous and structurally diverse non-fullerene acceptors (NFAs) have been developed in the last few years, and at the same time considerable progress has been made in the development of organic solar cells (OSCs).[1–3] NFAs with an acceptor–donor–acceptor (A–D–A) structure benefiting from adjustable energy levels, strong light absorptions, and reduced energy losses have increased the power conversion efficiency (PCE) record of OSCs to over 18%.[4]

The highly efficient A–D–A NFAs reported so far share the structural characteristic of each using a large multiple-ring-fused π-conjugated segment as the donor moiety in the core of the structure.[3,5] This feature endows the molecules with a completely planar central backbone and ensures a smooth flow from one end to the other for both π-electrons and charge carriers. Due to this feature together with the occurrence of strong intermolecular π–π stacking between the terminal A moieties, the molecules in the solid state can easily establish an effective three-dimensional charge-carrier transport network and thus generally display excellent charge mobility.[6] Moreover, the large fused D moiety often induces an efficient intramolecular charge transfer (ICT) to terminal A units, and thus enables an intense ICT band in the near-infrared (NIR) region and expands the wavelength range of the light absorption of the molecule to allow it to harvest more solar light.[7]

Undoubtedly, these fused-ring electron acceptors (FREAs) have achieved great success and have led the field into a new era with PCEs higher than 15%. However, the multiple-ring-fused core is relatively challenging to synthesize, and lacks much structural flexibility.[8] Therefore, besides FREAs, non-fused-ring acceptors (NFRAs) have also gained considerable attention and many such molecules have been designed and studied.[9–11] In order to improve the backbone planarity, elements that can produce intramolecular noncovalent interactions, such as O···S, O···H, and F···S, were designed into NFRA structures and have been demonstrated to be effective in producing a conformational lock and ultimately in enhancing the performance of the resulting devices.[12–14] However, such noncovalent interactions are generally weak and do not form to much of an extent in solution. Thus, in stark contrast to FREA molecules, NFRA molecules adopt twisted conformations in solution. During film formation procedures, NFRA molecules gradually stack together and planarize their backbones. But kinetic issues often prevent them from reaching the final fully planar stage, and instead keep them in various intermediate conformational stages.

In order to tackle this problem, we proposed here the use of bulky and "embracing"-type side chains to force two non-fused aromatic rings into planar conformations in both solution and

[a] Key Laboratory of Synthetic and Self-assembly Chemistry for Organic Functional Molecules, Center for Excellence in Molecular Synthesis, Shanghai Institute of Organic Chemistry, University of Chinese Academy of Sciences, Chinese Academy of Sciences, 345 Lingling Road, Shanghai 200032, P. R. China. E-mail: liws@mail.sioc.ac.cn

[b] I-Lab & Printable Electronics Research Centre, Suzhou Institute of Nano-tech and nano-bionics, Chinese Academy of Sciences, No. 398 Ruoshui Road, SEID, Suzhou Industrial Park, Suzhou, Jiangsu Province, 215123, P. R. China. E-mail: jfang2020@sinano.ac.cn

[c] CAS Key Laboratory of Energy Regulation Materials, Shanghai Institute of Organic Chemistry, Chinese Academy of Sciences, 345 Lingling Road, Shanghai 200032, China. E-mail: yaojh@mail.sioc.ac.cn

[d] Engineering Research Center of Zhengzhou for High Performance Organic Functional Materials, Zhengzhou Institute of Technology, 6 Yingcai Street, Huiji District, Zhengzhou, Henan 450044, P. R. China

† Electronic supplementary information (ESI) available. See DOI: 10.1039/d1tc05550j

Published on 31 January 2022. Downloaded by Suzhou Institute of Nano-Tech and Nano-Bionics, Chinese Academy of Sciences on 12/12/2022 2:15:21 AM.

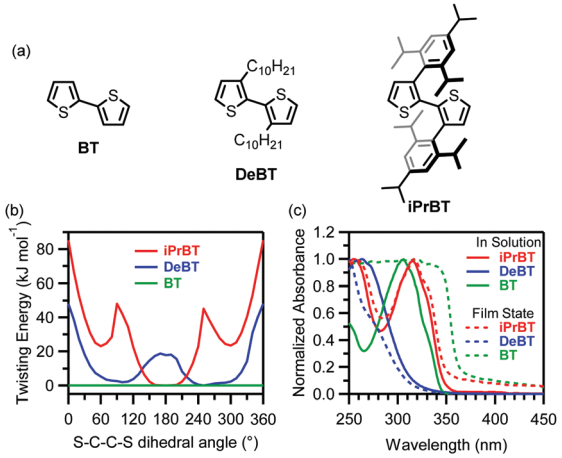

Fig. 1 (a) Chemical structures, (b) twisting energy profiles, and (c) UV-Vis absorption spectra in solution and film states of **BT**, **DeBT** and **iPrBT**.

film states. Non-fused bithiophene (**BT**) was shown—according to density functional theoretical (DFT) calculations at the B3LYP/6-31G level—to have essentially no energy barrier to twisting (Fig. 1b). In Fig. 1c, it also displayed an intense peak at a wavelength of about 306 nm in solution but a plateau in absorption for wavelengths up to 360 nm in the film state. This difference was attributed to the planarization of its conjugated backbone and intermolecular π–π stacking upon formation of the film. In comparison, the molecule **DeBT** having two decyl side chains at the 3,3′-positions showed an absorption peak at 255 nm in solution, blue shifted by 51 nm relative to that of **BT** in solution. Moreover, formation of the film state of **DeBT** coincided with a further blue shift of its main absorption peak. Note that DeBT in the film state also showed a newly present weak shoulder at about 275 nm (red shifted relative to the main peak). These observations suggested that the long alkyl chain substituents at the 3,3′-positions twisted the **BT** backbone in both the solution and film states, yielding a complicated description of twisting angles and multiple conformational stages. The results of DFT calculations were consistent with this picture, and showed the lowest energy state of **DeBT** involving S–C–C–S dihedral angles of about 90 or 270°. In contrast, when 2,4,6-triisopropylphenyl was used as the substituent at the 3,3′-positions, the resulting molecule, *i.e.*, **iPrBT**, displayed a light absorption peak at about 316 nm with very similar spectral shapes resulting from the solution and film states. This result indicated that the **iPrBT** molecule formed the same backbone configuration in solution and the film state. DFT calculations revealed the lowest energy state of the molecule resulting from a S–C–C–S dihedral angle of 180°, *i.e.*, an arrangement involving the two thiophene units in antiparallel coplanar positions. These observations can be reasonably explained as resulting from the isopropyl substituents at the 4,6-phenyl positions resembling two arms closely embracing the central thiophene units and forcing them to always stay in the antiparallel coplanar arrangement.

Inspired by the above thoughts and observations, we were encouraged to use **iPrBT** as a key building block in the place of multiple-ring-fused units for NFA design. Fig. 2 shows the subject of our first work, *i.e.*, **iPrBT-NFA**, which was used in combination with a benzothiadiazole bridge and 1,1-dicyanomethylene-3-indanone (IC) acceptor cap. The reference molecule **DeBT-NFA**, bearing the same chemical structure except the use of **DeBT** in place of **iPrBT**, was also designed and synthesized. Comparison studies found the embracing-type side chains in **iPrBT-NFA** as expected having great impacts on many optoelectronic properties as well as the film structure, and finally leading to a much-improved photovoltaic performance with an optimal PCE of 8.12% for **iPrBT-NFA** devices in contrast to the low PCE of only 0.29% for **DeBT-NFA** devices. Note that similar NFRAs bearing the same **iPrBT** core and achieving a PCE of 15.2% have been published during the time of this manuscript preparation.[15,16] In contrast to the reported molecules, **iPrBT-NFA** studied here was designed to use a benzothiadiazole bridge unit between IC and the **iPrBT** core to ensure an extension of its absorption band into the deep NIR region.

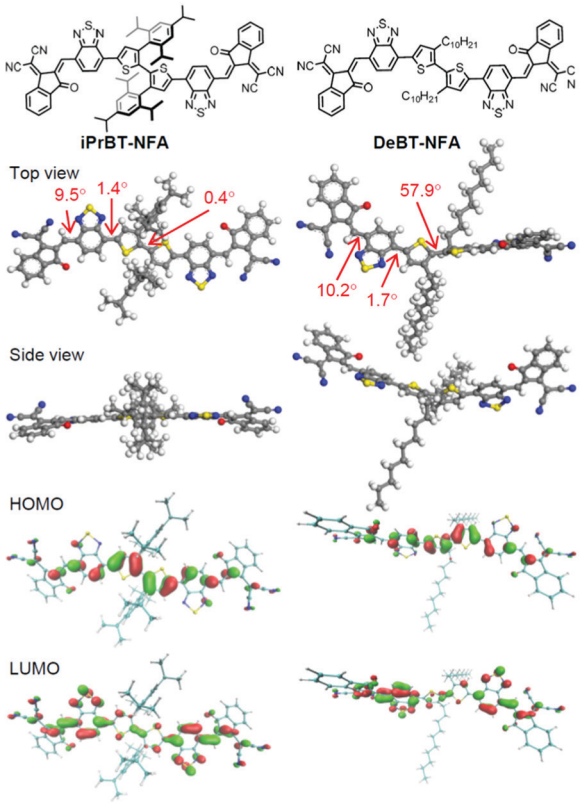

Fig. 2 Chemical structures, computed molecular geometry labelled with several important dihedral angles, and HOMO and LUMO orbitals of **iPrBT-NFA** and **DeBT-NFA**.

In order to check the rationale of the molecular design, DFT computations were first carried out at the B3LYP/6-31G level. As shown in Fig. 2, **iPrBT-NFA** was calculated to have an almost planar backbone with dihedral angles from the center to the terminus all near zero, specifically 0.4, 1.4, and 9.5°. Undoubtedly, this planar scaffold would facilitate π-electron communication throughout the entire backbone and lead to long-range delocalization of HOMO and LUMO orbitals. Meanwhile, the phenyl rings in the side chains were calculated to be

This journal is © The Royal Society of Chemistry 2022

Published on 31 January 2022. Downloaded by Suzhou Institute of Nano-Tech and Nano-Bionics, Chinese Academy of Sciences on 12/12/2022 2:15:21 AM.

perpendicular to the backbone with a dihedral angle of about 90°, a conformation preventing any significant conjugation of the phenyl units with the backbone and resulting in the phenyl units making no contribution to the formation of the highest occupied molecular orbital (HOMO) and lowest unoccupied molecular orbital (LUMO). This conformation was nevertheless found to be important due to its ensuring the isopropyl chains at its 4,6-positions behaving like two arms to tightly hold the backbone thiophene units and stop them from twisting. In comparison, **DeBT-NFA** was calculated to have a twisted backbone between the central thiophene units with a dihedral angle of about 57.9°—with the twisting causing HOMO electron density to mainly reside on the central segments, and LUMO electron density to be located on the terminal acceptor moieties.

Following this theoretical study, **iPrBT-NFA** and **DeBT-NFA** were synthesized following the schemes shown in Scheme S1. They both formed dark blue solids. Their chemical structures were unambiguously characterized by carrying out ^{1}H- and ^{13}C-NMR spectroscopic analyses, elemental analysis, and matrix-assisted laser desorption/ionization time-of-flight mass spectroscopy. **DeBT-NFA** displayed moderate solubility in common organic solvents such as chloroform and chlorobenzene, while **iPrBT-NFA** showed much better solubility.

Fig. 3a displays UV-Vis absorption spectra of **iPrBT-NFA** and **DeBT-NFA** in chloroform solutions and as thin films. In dilute chloroform solutions, **iPrBT-NFA** exhibited an absorption band in the wavelength range 500–800 nm with the strongest signal at 691 nm—while in comparison, **DeBT-NFA** showed a blue-shifted absorption band in the range 400–700 nm with the strongest signal at 576 nm. Considering the identical backbone structure for both molecules, this difference between their UV-Vis absorption spectra must have resulted from their different side chains at the central bithiophene unit. Unlike long alkyl side chains, that in general tend to twist backbones, the bulky and embracing-type side chains apparently helped the backbone stay in a coplanar structure and endowed the molecule with the ability to absorb more infrared light. In the film state, both molecules showed broadened and red-shifted absorption, attributed to the occurrence of intermolecular π–π stacking. Surprisingly, even with a much blue-shifted absorption band in solution, **DeBT-NFA** was found to extend its absorption edge in the film state more so than did **iPrBT-NFA**. Consequently, the

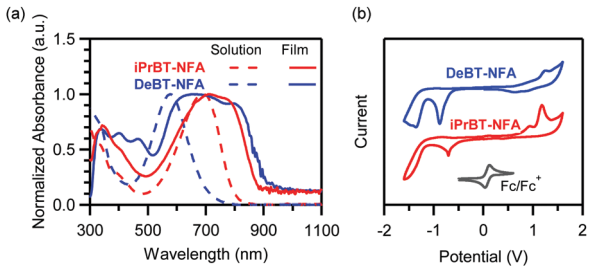

Fig. 3 (a) UV-Vis absorption spectra in a chloroform solution and film state and (b) CV profiles of **iPrBT-NFA** and **DeBT-NFA**.

iPrBT-NFA film showed a light-absorption onset point at 870 nm, while **DeBT-NFA** film exhibited it at about 910 nm. This result indicated a narrower bandgap for the **DeBT-NFA** film than for the **iPrBT-NFA** film (1.36 *vs.* 1.42 eV). At the same time, we noticed much broader absorption bands for the **DeBT-NFA** film than for the **iPrBT-NFA** film. These observations suggested that backbone planarization took place during the formation of the **DeBT-NFA** film. However, this process proceeded neither comprehensively nor completely, resulting in multiple conformational stages for **DeBT-NFA** molecules. We considered it reasonable to deduce that some **DeBT-NFA** molecules fully planarized their backbones and closely π–π stacked together, giving rise to light absorption at the red edge. But most **DeBT-NFA** molecules apparently still kept their backbones twisted and were poor in π–π stacking, features favorable neither for charge transport nor for photovoltaic performance.

Cyclic voltammetry (CV) was used to determine energy levels of the HOMO and LUMO orbitals of the molecules. As shown in Fig. 3b, both **iPrBT-NFA** and **DeBT-NFA** films displayed irreversible reduction and oxidation peaks in the negative and positive voltage scannings, respectively. From the oxidation onset ($E_{\text{onset, ox}}$) and reduction onset ($E_{\text{onset, red}}$) potentials of these peaks, the HOMO and LUMO energy levels of **iPrBT-NFA** and **DeBT-NFA** were calculated to be −5.50/−4.10 and −5.39/−4.01 eV. **DeBT-NFA** clearly exhibited shallower-lying HOMO and LUMO energy levels than did **iPrBT-NFA**, implying some impact of backbone planarity.

Using **PM6** (Fig. S15, ESI†) as a donor component, the photovoltaic performances of **iPrBT-NFA** and **DeBT-NFA** as acceptor components were investigated with an ITO/PEDOT:PSS/active layer/PFN-Br/Al device configuration. In optimization experiments, both devices achieved their optimal performances when prepared by spin-coating pre-mixed **PM6:NFA** chloroform solutions with a **PM6** concentration of 7 mg mL^{-1}, a D/A ratio of 1/1.6, and 0.75% 1,8-diiodooctane (DIO) as additive at 3700 rpm, and subsequently carrying out thermal annealing at 100 °C for 5 minutes (Tables S1–S6, ESI†). As shown in Fig. 4a, the optimal **iPrBT-NFA** device performance involved a V_{oc} of 0.74 V, J_{sc} of 17.72 mA cm^{-2} and FF of 61.8%, giving the best PCE of 8.13%. But **DeBT-NFA** devices showed extremely poor performance, with an optimized PCE of only 0.29% (V_{oc} = 0.77 V, J_{sc} = 1.23 mA cm^{-2}, FF = 30.9%). An external quantum efficiency (EQE) spectroscopy investigation found that **iPrBT-NFA** devices normally worked in the wavelength range 300–900 nm with a maximum of 61.7% at 610 nm (Fig. 4b), while **DeBT-NFA** devices showed poor photoresponsiveness in both visible and infrared regions.

In order to understand the origin of this large difference in performance, hole and electron mobility (μ_h and μ_e) levels of the active layers were measured using the space charge-limited current (SCLC) method with hole-only ITO/PEDOT:PSS/active layer/Au and electron-only ITO/ZnO/active layer/Ca/Al devices (Fig. 4c and d). The μ_h and μ_e of the **PM6/iPrBT-NFA** active layer were measured to be 4.34×10^{-4} and 1.13×10^{-4} cm^2 V^{-1} s^{-1}, respectively, both two orders of magnitude greater than those of the **PM6/DeBT-NFA** active layer (1.66×10^{-6} and $2.25 \times$

Published on 31 January 2022. Downloaded by Suzhou Institute of Nano-Tech and Nano-Bionics, Chinese Academy of Sciences on 12/12/2022 2:15:21 AM.

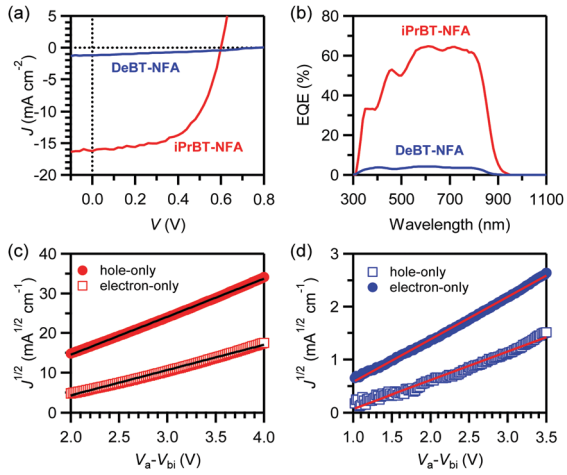

Fig. 4 (a) J–V curves and (b) EQE spectra of the optimal **iPrBT-NFA** and **DeBT-NFA** devices. (c and d) $J^{1/2}$–V plots of hole-only and electron-only devices based on (c) **PM6/iPrBT-NFA** and (d) **PM6/DeBT-NFA**.

10^{-6} cm^2 V^{-1} s^{-1}). Moreover, an atomic force microscopy (AFM) investigation revealed the **PM6/iPrBT-NFA** film having shown a homogeneous microphase separation morphology and a smooth surface with a root-mean-square (RMS) roughness of 3.85 nm (Fig. 5a and b). In sharp contrast, clear fibrous objects with widths of hundreds of nanometers were observed in the **PM6/DeBT-NFA** film. These features made the film non-uniform and very rough, with an RMS roughness of 39.21 nm. Obviously, such a morphology is in general not favorable for photovoltaic performance.

Furthermore, two-dimensional grazing-incidence wide-angle X-ray scattering (2D-GIWAXS) experiments on the molecules were conducted to study their respective packings and orientations (Fig. 5c and d). The neat **DeBT-NFA** film yielded (100) and (200) diffraction peaks at 0.31 and 0.64 Å^{-1}, respectively, in both out-of-plane (OOP) and in-plane (IP) directions, suggesting a lamellar structure with a distance between layers of 20.5 Å. A weak (010) diffraction peak was identified at 1.76 Å^{-1}, corresponding to a π–π stacking distance of 3.57 Å. Similarly, the neat **iPrBT-NFA** film exhibited a set of (100), (200) and (010) diffraction peaks from a lamellar structure with a distance between layers of 17.0 Å and π–π stacking distance of 3.55 Å. While these peaks were observed to be weaker than those of **DeBT-NFA**, they were still clear observations, and their shorter d-spacings demonstrated that the bulky and embracing-type side chains in **iPrBT-NFA** did not prevent intermolecular π–π stacking from occurring. Considering the great steric hindrance involved here, such π–π stacking must have occurred between terminal benzothiadiazole and IC moieties of neighboring molecules. This conclusion was consistent with those of most reported NFAs having A–D–A structures. For **PM6:iPrBT-NFA** and **PM6:DeBT-NFA** blend films, a (100) diffraction peak appeared only in the OOP direction, at positions similar to those for the neat films, indicating an edge-on-dominated molecular orientation in both blend films. Notably, **PM6:iPrBT-NFA** blend films displayed additional diffraction

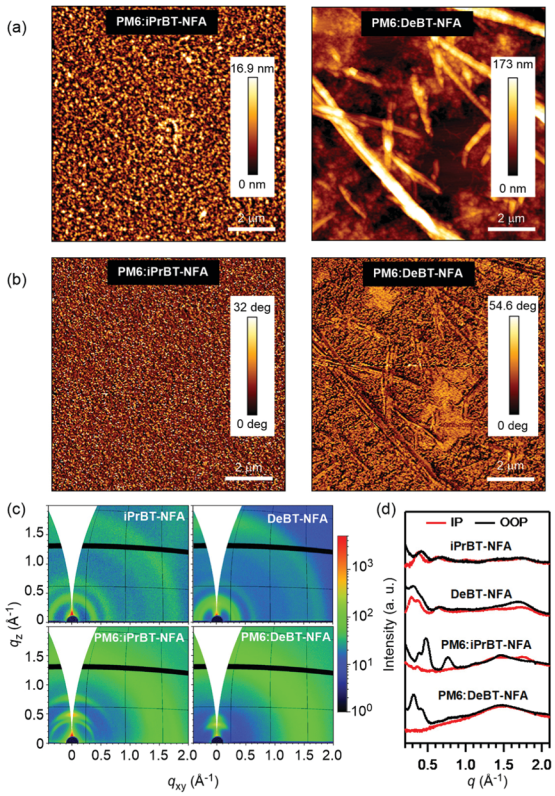

Fig. 5 (a) AFM height and (b) AFM phase images of of **PM6/iPrBT-NFA** and **PM6/DeBT-NFA** films. (c) 2D GIWAXS patterns and (d) scattering profiles in out-of-plane and in-plane directions of **iPrBT-NFA** and **DeBT-NFA** neat films and **PM6:iPrBT-NFA** and **PM6:DeBT-NFA** blend films.

peaks at 0.49 and 0.77 Å^{-1} in the OOP direction, probably originating from the **PM6** crystallization. Further, in the IP direction, the π–π-stacking peak still appeared at 1.77 Å^{-1}. But none of these peaks were not observed for the **PM6:DeBT-NFA** blend film. These results as well as the AFM results showed a much better molecular packing structure and morphology for the **PM6:iPrBT-NFA** blend film than for the **PM6:DeBT-NFA** blend film.

The dependences of V_{oc} and J_{sc} on light intensity (P_{light}) were investigated to gain insight into the charge recombination mechanism in the **iPrBT-NFA** devices. As shown in Fig. 6a, V_{oc} was found to linearly increase with P_{light}, with a slope of 1.10 kT q^{-1}, suggesting the occurrence of Shockley-Read-Hall recombination to some degree.[17] In general, J_{sc} depends on P_{light} according to the relationship $J_{sc} \propto P_{light}^{\alpha}$, where the power law index α reflects the extent of bimolecular recombination; an α value near 1 is indicative of the device exhibiting effective exciton transport and reduced energy loss caused by bimolecular recombination. In this work, we obtained an α value of 0.97, suggesting the effective suppression of bimolecular recombination in **iPrBT-NFA** devices. Furthermore, analysis of the dependence of photocurrent density (J_{ph}) on effective voltage (V_{eff}), shown in Fig. 6b, indicated a saturated photocurrent density (J_{sat}) of 18.53 mA cm^{-2} for the devices. Based on these measurements, the ratio of photocurrent against this

This journal is © The Royal Society of Chemistry 2022

Published on 31 January 2022. Downloaded by Suzhou Institute of Nano-Tech and Nano-Bionics, Chinese Academy of Sciences on 12/12/2022 2:15:21 AM.

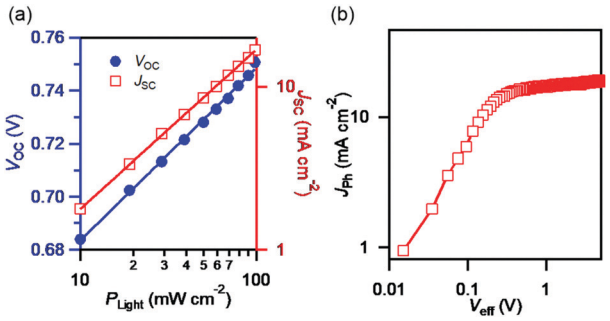

Fig. 6 (a) Plots of V_{OC} and J_{SC} *versus* light intensity and (b) a J_{Ph}–V_{eff} curve of **PM6/iPrBT-NFA** devices.

saturated value under the short-circuit condition was calculated to be 94.1%, reflecting a good charge separation efficiency. However, the photocurrent ratio dropped to 76.8% under the maximum power output condition, suggesting a poor charge collection efficiency for the devices.

In summary, we demonstrated here the use of bulky and "embracing"-type side chains in photovoltaic material design. In contrast to **DeBT-NFA** carrying conventional long alkyl side chains, **iPrBT-NFA** functionalized with two arm-like 2,4,6-tripropylphenyl side chains showed a planar backbone structure even in solution, and thus leading to a red-shift absorption band in solution. The bulky side chains in **iPrBT-NFA**, although changing the molecular packing structure, did not hamper π–π stacking of terminal acceptor moieties. Regarding the blending of **iPrBT-NFA** with **PM6** for OSC fabrication, the so-formed active layers were observed to display a good morphology with appropriate microphase separation and large charge mobility, thus affording a PCE of 8.13% for the optimized device. Therefore, exemplified by **iPrBT-NFA**, the work has paved the way to a new method for achieving a coplanar backbone structure, in addition to previous methods involving ring fusion and intramolecular non-covalent configuration locks. Although the photovoltaic performance resulting from the use of **iPrBT-NFA** still lags behind the-state-of-the-art level, the strategy developed merits further investigation and application.

Conflicts of interest

The authors declare no conflicts of competing interest.

Acknowledgements

We are grateful for the financial support from the National Natural Science Foundation of China (No. 21674125, 21672251, 21975279 and 51761145043), Strategic Priority Research Program of the Chinese Academy of Sciences (No. XDB20020000), Shanghai Institute of Organic Chemistry (No. sioczz202123), and Zhengzhou Institute of Technology.

Notes and references

1 Y. Tong, Z. Xiao, X. Du, C. Zuo, Y. Li, M. Lv, Y. Yuan, C. Yi, F. Hao, Y. Hua, T. Lei, Q. Lin, K. Sun, D. Zhao, C. Duan, X. Shao, W. Li, H.-L. Yip, Z. Xiao, B. Zhang, Q. Bian, Y. Cheng, S. Liu, M. Cheng, Z. Jin, S. Yang and L. Ding, *Sci. China: Chem.*, 2020, **63**, 758–765.
2 A. Armin, W. Li, O. J. Sandberg, Z. Xiao, L. Ding, J. Nelson, D. Neher, K. Vandewal, S. Shoaee, T. Wang, H. Ade, T. Heumüller, C. Brabec and P. Meredith, *Adv. Energy Mater.*, 2021, **11**, 2003570.
3 C. Yan, S. Barlow, Z. Wang, H. Yan, A. K. Y. Jen, S. R. Marder and X. Zhan, *Nat. Rev. Mater.*, 2018, **3**, 18003.
4 Q. Liu, Y. Jiang, K. Jin, J. Qin, J. Xu, W. Li, J. Xiong, J. Liu, Z. Xiao, K. Sun, S. Yang, X. Zhang and L. Ding, *Sci. Bull.*, 2020, **65**, 272–275.
5 S. Dey, *Small*, 2019, **15**, 1900134.
6 D. Li, X. Zhang, D. Liu and T. Wang, *J. Mater. Chem. A*, 2020, **8**, 15607–15619.
7 H. Wang, J. Cao, J. Yu, Z. Zhang, R. Geng, L. Yang and W. Tang, *J. Mater. Chem. A*, 2019, **7**, 4313–4333.
8 X. Li, F. Pan, C. Sun, M. Zhang, Z. Wang, J. Du, J. Wang, M. Xiao, L. Xue, Z.-G. Zhang, C. Zhang, F. Liu and Y. Li, *Nat. Commun.*, 2019, **10**, 519.
9 Z.-P. Yu, Z.-X. Liu, F.-X. Chen, R. Qin, T.-K. Lau, J.-L. Yin, X. Kong, X. Lu, M. Shi, C.-Z. Li and H. Chen, *Nat. Commun.*, 2019, **10**, 2152.
10 S. Li, L. Zhan, F. Liu, J. Ren, M. Shi, C.-Z. Li, T. P. Russell and H. Chen, *Adv. Mater.*, 2018, **30**, 1705208.
11 H. Huang, Q. Guo, S. Feng, C. E. Zhang, Z. Bi, W. Xue, J. Yang, J. Song, C. Li, X. Xu, Z. Tang, W. Ma and Z. Bo, *Nat. Commun.*, 2019, **10**, 3083.
12 Y. N. Chen, M. Li, Y. Wang, J. Wang, M. Zhang, Y. Zhou, J. Yang, Y. Liu, F. Liu, Z. Tang, Q. Bao and Z. Bo, *Angew. Chem., Int. Ed.*, 2020, **59**, 22714–22720.
13 B.-S. Lu, Y. Zhang, T.-Y. Hu, Y.-F. Ma, Y.-N. Zhu, D.-W. Liu, Z.-Q. Zhang, E. Wang, W. Ma and H.-L. Zhang, *Org. Electron.*, 2021, **93**, 106132.
14 J. Gao, Y. Li, S. Li, X. Xia, X. Lu, M. Shi and H. Chen, *Solar Energy Mater. Sol. Cells*, 2021, **225**, 111046.
15 L. Ma, S. Zhang, J. Zhu, J. Wang, J. Ren, J. Zhang and J. Hou, *Nat. Commun.*, 2021, **12**, 5093.
16 P. Bi, S. Zhang, J. Ren, Z. Chen, Z. Zheng, Y. Cui, J. Wang, S. Wang, T. Zhang, J. Li, Y. Xu, J. Qin, C. An, W. Ma, X. Hao and J. Hou, *Adv. Mater.*, DOI: 10.1002/ADMA.202108090.
17 S. R. Cowan, A. Roy and A. J. Heeger, *Phys. Rev. B: Condens. Matter Mater. Phys.*, 2010, **82**, 245207.